A Complete Sample of Soft X-ray Selected AGN: II. Statistical Analysis[1]

Dirk Grupe[2]
Astronomy Department, Ohio State University, 140 W. 18th Ave., Columbus, OH-43210, U.S.A.
dgrupe@astronomy.ohio-state.edu

ABSTRACT

Direct correlations and a Principal Component Analysis (PCA) are presented for a complete sample of 110 soft X-ray selected AGN of which about half are Narrow-Line Seyfert 1 galaxies (NLS1s). The direct correlation analyses show that narrower FWHM(Hβ) correlates with steeper X-ray spectrum, stronger optical FeII emission, weaker [OIII] emission and stronger short-term X-ray variability. This direct correlation analysis and the PCA confirm the Boroson & Green (1992) Eigenvector 1 relationship for AGN: FeII strength anti-correlates with [OIII] line strength. Eigenvector 1 is well-correlated with the Eddington luminosity ratio $L/L_{\rm Edd}$ while Eigenvector 2 shows a very good correlation with the mass of the central black hole $M_{\rm BH}$ and the mass accretion rate $\dot{M}$. The Eddington ratio $L/L_{\rm Edd}$ correlates with the X-ray spectral index $\alpha_{\rm X}$ and the black home mass $M_{\rm BH}$ anti-correlates with the X-ray variability χ^2/ν. The Eddington ration $L/L_{\rm Edd}$ may be interpreted as the age of an AGN: AGN with steep X-ray spectra, strong FeII, and weak [OIII] are AGN in an early phase of their evolution. In this hypothesis NLS1s are young AGN.

Subject headings: galaxies: active - quasars:general

1. Introduction

The ROSAT All-Sky Survey (RASS, Voges et al. (1999)) led to the discovery of a large number of previously unknown AGN. While being non-prominent at other wavelengths these sources are bright at soft X-ray energies. Following the selection criteria described in Thomas et al. (1998) and Grupe et al. (2001a, 2004) led to a total of 113 bright soft X-ray selected AGN. Half of these AGN are Narrow-Line Seyfert 1 galaxies (NLS1s, Osterbrock & Pogge (1985)) which are characterized by their relatively narrow Hβ emission lines from the Broad Line Region (BLR), their strong optical FeII emission and weak emission from forbidden lines from the Narrow Line Region (NLR). NLS1s are the class of AGN with the steepest X-ray spectra (e.g. Puchnarewicz et al. (1992); Boller et al. (1996); Brandt et al. (1997); Grupe et al. (1998a, 2001a); Williams et al. (2003)). NLS1 appear to be more common among soft X-ray selected AGN compared with optically selected samples (e.g. Stephens (1989); Edelson et al. (1999); Grupe (1996); Grupe (2000) and references therein).

It has been shown by e.g. Laor et al. (1994, 1997), Grupe (1996); Grupe et al. (1999b), Sulentic et al. (2000), and Vaughan et al. (2001) that the width of the BLR Hβ line, the strength of FeII and the strength of the NLR [OIII] emission are linked to the X-ray spectral index $\alpha_{\rm X}$[3]: A larger $\alpha_{\rm X}$ goes with an increase of the FeII strength and decrease of the Hβ width and [OIII]

[1]Based in part on observations at the European Southern Observatory La Silla (Chile) with the 2.2m telescope of the Max-Planck-Society during MPI and ESO time and the ESO 1.52m telescope during ESO time in September 1995 and September 1999.

[2]Guest observer, McDonald Observatory, University of Texas at Austin

[3]Throughout the paper the spectral indeces are energy spectral induces defined by $F_\nu \propto \nu^{-\alpha}$.

strength. All these relationships can be described by one basic underlying parameter, often called Eigenvector 1 or the First Principal Component. Boroson & Green (1992) examined the properties of a sample 87 bright PG quasars and found from a Principal Component Analysis (PCA) that Eigenvector 1 correlates with the strength of FeII and anti-correlates with the strength of the [OIII] emission. Boroson (2002) and Sulentic et al. (2000) suggested that Eigenvector 1 is the luminosity to Eddington luminosity ratio $L/L_{\rm Edd}$. This relationship has been clearly demonstrated by the study of Yuan & Wills (2003) of high-redshift quasars. Grupe (1996) and Grupe et al. (1999b) suggested that Eigenvector 1 might represent the 'age' of AGN and that in this picture NLS1s are AGN in an early phase of their evolution, a conclusion that has also been drawn for high-redshift quasars and some Broad Absorption Line Quasars (Mathur (2000); Becker et al. (2000)). The second larges Eigenvector in the Boroson & Green (1992) sample seems to be the mass accretion rate $\dot{M}$ (Boroson 2002).

I have studied a sample of 113 soft X-ray AGN selected from the RASS. The RASS and pointed ROSAT Position Sensitive Proportional Counter (PSPC, Pfeffermann et al. (1987)) and High Resolution Imager (HRI) observations of this sample have been described in detail by Grupe et al. (2001a). The objects were selected to be X-ray bright (CR$\geq$0.5 PSPC cts s^{-1}) at high galactic latitude (—b—$>$ 20°) and having a soft X-ray spectrum (hardness ratio HR$\leq$0.0; Grupe et al. (2001a) and Grupe et al. (2004)). The sample is complete for all AGN following these selection criteria. It is also complete with respect to that X-ray and optical spectra exist for each source. Even though the sample is X-ray selected it does not miss any optical counterpart. X-ray and optical properties can be measured in the same way for each object. The sample presented here excludes the known X-ray transient sources IC 3599, WPVS007 and RX J1624.9+7554 (Brandt et al. (1995); Grupe et al. (1995a,b, 1999a)) leaving 110 objects in the current sample. Even though the sample is complete following the selection criteria given above, it is biased towards unabsorbed, bright, and low-redshift sources. Only a few sources of the sample show significant optical reddening and X-ray absorption (Grupe et al. 1998b). The sample misses faint and/or absorbed X-ray sources. X-ray absorption by neutral elements not only reduces the observed flux, but because the sample was selected by hardness ratio, it also converts a source into a hard X-ray source even though its intrinsic X-ray spectrum may be steep. As shown recently by Williams et al. (2003) there is a large number of NLS1s derived from the Sloan Digital Sky Survey (SDSS, York et al. (2000)) which do not show significant X-ray emission. These sources may be either intrinsically X-ray weak or are strongly absorbed by neutral elements. Another bias comes from the absorption of neutral elements in our Galaxy. Even though the sample was selected by high-galactic latitude objects, it still misses borderline objects which may be intrinsically not absorbed, but become 'hard' X-ray sources because of the Galactic absorption in the soft X-ray band. By extending the sample towards fainter and absorbed sources, the immediate effect on the sample would be a reduced fraction of NLS1s as discussed in Grupe (2000). However, missing fainter and/or absorbed objects does not affect the results presented and discussed in this paper.

Optical spectra were obtained at McDonald Observatory, ESO La Silla, CTIO, and the TLS Tautenburg and the observations, the data reduction, and the line measurements are described in detail in Grupe et al. (2004) (Paper I). In Paper I we presented all spectra that have not been published before, performed a simple statistical analysis of the data and showed the distributions of optical and X-ray properties among NLS1s and Broad Line Seyfert 1s (BLS1s). NLS1s and BLS1s were defined following the definition of Goodrich (1989) with NLS1s being AGN with FWHM(Hβ)$\leq$2000 km s^{-1} and BLS1s with FWHM(Hβ)$>$2000 km s^{-1}.

In the soft X-ray selected sample we found that NLS1s and BLS1s have different distributions of their rest frame equivalent width EW(FeII), FeII/Hβ ratio, $\alpha_{\rm X}$, and X-ray variability. NLS1s have on average the highest EW(FeII) and FeII/Hβ ratios, the steepest X-ray spectra and are more variable than BLS1s. In this sample they have similar distributions in their redshifts, luminosities, and EW(Hβ). $\alpha_{\rm X}$ was determined from a powerlaw model with Galactic absorption of neutral elements to the RASS spectra (Grupe

et al. 2001a) with column densities $N_{\rm H,gal}$ given by Dickey & Lockman (1990). $\alpha_{\rm X}$ is independent of $N_{\rm H}$ and NLS1s and BLS1s have similar distributions of their Galactic $N_{\rm H}$ values.

The black hole masses were estimated from the monochromatic luminosity at 5100Å and FWHM(Hβ) listed in Table 2 in Grupe et al. (2004) using the relationships given in Kaspi et al. (2000) by determining the size of the BLR by $R_{\rm BLR} \propto \lambda L_{5100}^{0.7}$ and the mass of the black hole by $M_{\rm BH} \propto R_{\rm BLR} \times FWHM({\rm H}\beta)$. These black hole masses were used to determine the Eddington luminosities. The rest frame bolometric luminosities $L_{\rm bol}$ were estimated from a power law model with exponential cutoff (see Figure 2 in Grupe et al. (2004)) to the optical and X-ray data. The Eddington and bolometric luminosities given here are approximate. An analysis of the black hole masses of the sample objects shows that for a given luminosity NLS1 have smaller black hole masses than BLS1s and that the Magorrian et al. (1998) and Tremaine et al. (2003) $M_{\rm BH} - \sigma$ relationship between the black hole mass and galaxy bulge stellar velocity dispersion does not apply for most NLS1s (Grupe & Mathur (2004)).

In this paper I present the statistical analysis of the complete sample of 110 soft X-ray selected AGN defined and presented in Paper I. The paper is organized as follows: In § 2 the data analysis, especially the PCA, is explained, in § 3 the results of the statistical analysis are presented, followed by a discussion in § 4. Luminosities are calculated assuming a Hubble constant of H_0 =75 km s^{-1}Mpc^{-1} and a deceleration parameter of q_0 = 0.0.

2. Data analysis

The correlation analysis presented in this paper uses the Spearman rank order and the Student's t-test to check the significance of the correlation. The advantage of the Spearman rank order analysis compared with a correlation analysis on the direct measurements is that outliers do not affect the results as much plus the correlation coefficient is not as strongly affected if the correlation is not a linear function.

One main aspect of this paper is the Principal Component Analysis of the data. The idea behind this method is to reduce the number of parameters to describe a source from many to a few relevant parameters. The mathematical formalism behind the PCA is linear algebra to find the Eigenvalues and Eigenvectors for the correlation coefficients matrix. It is not the task of this paper to describe this method in detail. An excellent description of how PCA works can be found in Francis & Wills (1999).

3. Results

3.1. Correlation Analysis

Table 1 contains the Spearman rank order correlation coefficients between FWHM(Hβ) and [OIII]λ5007Å, the equivalent widths (EW) of Hβ, [OIII] and the FeIIλ4570Å blend, the flux ratios [OIII]/Hβ and FeII/Hβ, $\alpha_{\rm X}$, the 0.2-2.0 kev rest-frame X-ray luminosity and the soft X-ray variability parameter χ^2/ν. There are five rows in the table for each observational property, in the following order: the whole sample (110 sources), high-luminosity sources with log $L_{\rm X}$ >37.0 [W] (57), low-luminosity objects with log $L_{\rm X}$ <37.0 [W] (53), NLS1 (51), and BLS1s (59). The part below the diagonal displays the Spearman rank order correlation coefficient $r_{\rm S}$ and the part above the diagonal shows the value $t_{\rm S}$ from a Student's t-test to indicate the significance of the correlation. All correlations with $t_{\rm S}$> 3.0 are shown as bold face. A $t_{\rm S}$=3.0 for 110 source is equivalent to a probability P<0.1% of a random distribution. For the NLS1s, BLS1s, low-luminosity, and high-luminosity subsamples with their 50-60 sources a $t_{\rm S}$=3.0 is equivalent to P<0.2%. In the following the most important correlations are presented.

3.1.1. FWHM(Hβ) and $\alpha_{\rm X}$

Figure 1 displays the well-known relationship between FWHM(Hβ) and $\alpha_{\rm X}$, namely that objects with steep X-ray spectra appear to have relatively narrow BLR emission lines. This relationship has been established for many optically and X-ray selected samples (e.g. Boller et al. (1996); Grupe (1996); Laor et al. (1994, 1997); Grupe et al. (1999b); Vaughan et al. (2001)). In our complete sample the FWHM(Hβ) and $\alpha_{\rm X}$ are well-correlated with a Spearman rank order correlation coefficient $r_{\rm S}$=–0.49 with a Student's t-test $t_{\rm S}$=–5.34. As noted by Grupe et al. (1999b) and Vaughan et al. (2001) this correlation im-

proves when only the high-luminosity sources are considered. In the current sample, r_S increases to –0.63 with t_S=–6.01. (Table 1). When only the low-luminosity sources are taken into account, the correlations significantly decreases to r_S=–0.41 with t_S=–3.18. It is interesting to note that the FWHM(Hβ)-α_X anti correlation can be seen only when NLS1 and BLS1s are both included When the two groups are examined separately, the correlations seems to vanish. This is in agreement with the results of Xu et al. (2003) for 155 BLS1s for which there was no correlation found between FWHM(Hβ) and α_X for their sample. The reason is that the ranges in FWHM(Hβ) become to small to have a large enough 'lever-arm' to detect any significant correlation.

3.1.2. [OIII] and FeII

Boroson & Green (1992) found one of the best-known relationships among the observational properties of AGN: the strength of the FeII emission anti-correlates with the [OIII] strength (see also § 3.2). This relation has been found in many optically selected samples of low-redshift AGN (e.g. Vaughan et al. (2001); Xu et al. (2003)) and most recently even in a sample of high-redshift quasars by Yuan & Wills (2003). In the sample presented here, this trend is clearly confirmed. Figure 2 shows the anti correlations between the EW([OIII]) and EW(FeII) (left) an the FeII/Hβ ratio (right). For the whole sample the Spearman rank order correlation coefficients are r_S=–0.28 with t_S=–2.98 and r_S=–0.37 with t_S=–4.11, respectively. These anti correlations become even stronger among the high luminosity sources (Table 1). The [OIII] - FeII anti-correlation is even stronger between EW(FeII) and the [OIII]/Hβ line flux ratio with r_S=–0.45 and t_S=–5.23. Figure 3 displays this relation.

3.1.3. Hβ and FeII

As noticed by e.g. Boroson & Green (1992), Sulentic et al. (2002), and Zheng et al. (2002) and most recently by Marziani et al. (2003) and Stepanian et al. (2003) there is an anti-correlation between the FWHM(Hβ) and the EW(FeII) and FeII/Hβ flux ratio. Also the AGN of the soft X-ray selected sample show these anti-correlations (Figure 4). The anti-correlation between FWHM(Hβ) and the FeII/Hβ flux ratio is the strongest among independent properties in the whole sample with r_S=–0.71 and t_S=–10.5. This anti-correlations remains this strong even if the sample is split into a low-luminosity and high-luminosity subsample. The FWHM(Hβ) - EW(FeII) anti-correlation is strong for the whole sample with r_S=–0.49 and t_S=–5.84 and slightly stronger among the high-luminosity objects with r_S=–0.63 and t_S=–6.05. Interestingly, NLS1s and BLS1s show opposite correlations of FWHM(Hβ) and EW(FeII): while for NLS1s the EW(FeII) increases with Hβ line widths, the EW(FeII) decreases with Hβ line widths for the BLS1s. For the whole sample, the right panel in Figure 4 shows a peak in EW(FeII) at around FWHM(Hβ) ≈2000km s^{-1}.

3.1.4. α_X and FeII and [OIII] relations

α_X does not only show an anti-correlation with FWHM(Hβ) (§ 3.1.1) it also correlates with the EW(FeII) and the FeII/Hβ line ratio. This relation was discovered by Wilkes et al. (1987) and has been found in a number of samples e.g. by Laor et al. (1994, 1997) and Vaughan et al. (2001). Figure 5 displays these relations. The α_X - EW(FeII) correlation is strong with r_S=+0.55 and t_S=+6.87 for the whole sample and stays no matter how the sample is split (see Table,1). The correlation between α_X and the FeII/Hβ flux ratio is weaker with r_S=+0.40 and t_S=+4.57, but still significant.

As shown is §3.1.2 there is an anti-correlation between the strengths of the [OIII]λ5007 line and the 4570ÅFeII blend. This result suggests that α_X should be anti-correlated with the [OIII] line strength and indeed there is as shown in Figure 6. α_X is anti-correlated to the EW([OIII]) with r_S=–0.31 and t_S=–3.34 and to the [OIII]/Hβ ratio with r_S=–0.40 and t_S=–4.53. A similar result has been reported previously by e.g. Vaughan et al. (2001).

3.1.5. Log L_X vs. α_X

NLS1s show a strong correlation between the rest-frame 0.2-2.0 keV X-ray luminosity and α_X (Fig. 7) with r_S=0.63 and t_S=5.7. This result confirms the findings by Laor et al. (1994) and Grupe et al. (1999b) and most recently by Williams et al. (2004). As shown in Fig. 7 and Table 1, this correlation is not present among BLS1s.

3.1.6. log L_X and [OIII]

As noticed by Grupe (1996) and Grupe et al. (1999b), the luminosity of the sources correlates with the FWHM([OIII]) and anti-correlates with the [OIII]/Hβ line ratio. As displayed in Figure 8 these relations appear to be present in the current sample. The correlation between the 0.2-2.0 soft X-ray luminosity and FWHM([OIII]) is rather strong with r_S=+0.46 and t_S=+5.41 and appears to be of similar significance among NLS1s and BLS1s (see Table 1). The log L_X - [OIII]/Hβ anti-correlation is weaker, but present with r_S=–0.33 and t_S=–3.60.

3.1.7. Correlations among luminosities

Figure 9 displays the rest frame 0.2-2.0 keV X-ray luminosity L_X vs. the bolometric luminosity L_{bol} and the rest frame monochromatic luminosity at 5100 Å $\lambda L_{5100\mathring{A}}$. Figure 9 also shows the regression curves through the data with the following relationships:

$$log\ L_{bol} = (0.44 \pm 2.30) + (1.02 \pm 0.06) \times log\ L_X \quad (1)$$

and

$$log\ \lambda L_{5100\mathring{A}} = (2.66 \pm 0.93) + (0.93 \pm 0.05) \times log\ L_X \quad (2)$$

Note that because the EUV part of the AGN Spectral Energy Distribution is unobservable it leaves large uncertainties in estimating the bolometric luminosities (e.g. Elvis et al. (1994)). Therefore the equations given above can only be used for rough estimates.

3.1.8. Correlations with X-ray variability

Figure 10a displays the X-ray variability parameter χ^2/ν vs. X-ray rest frame X-ray luminosity (see also Grupe et al. (2001a)). For the whole sample there is a light anti correlation with r_S=–0.28 with t_S=–2.81. This result confirms the findings of e.g. Barr & Mushotzky (1986); Lawrence & Papadakis (1993); Green et al. (1993) and Leighly (1999) that sources with higher luminosity tend to be less variable than low-luminosity sources.

Figure 10b shows the anti correlation between χ^2/ν and FWHM(Hβ) for the whole sample this relationship is anti correlated with r_S=–0.34 with t_S=–3.73. As shown in the distribution of χ^2/ν (Figure 10 in Grupe et al. (2004)) NLS1s tend to be more variable in soft X-rays than BLS1s. This confirms the findings of Leighly (1999) that for a given luminosity NLS1s are more variable than BLS1s, and Wandel & Boller (1998) who found a correlation of the FWHM(Hβ) with the X-ray doubling time scales.

The X-ray variability χ^2/ν was derived from the RASS light curves (Grupe et al. 2001a). Keep in mind that χ^2/ν is not only a function of variability but also of signal-to-noise. Our estimates of the variability parameter χ^2/ν take the errors from the instrumental background and photon noise into account (Grupe et al. 2001a). The contribution of noise to the light curve of a single source depends on how bright the source was and how long the RASS scan was. Brighter sources observed during a longer RASS scan (≈30s) have an error from photon noise typically in the order of 10% while for fainter sources during a shorter scan (≈10s) the error is typically in the order of 30-40%. However, because the sample is selected by count rate and most sources have count rates between 0.5-2.0 PSPC cts s^{-1} and they were all observed in the same way during the RASS, the contribution of noise to the source signal is about the same in each source. This means that noise can affect the result for a single source, but not statistically for the whole sample. If the variability is due to noise it would be visible if the sources with lower count rates are more variable (larger χ^2/ν) than the sources with larger count rates. A check between the RASS count rate and χ^2/ν shows that this is not the case.

3.2. Principal Component Analysis

A PCA was performed for the following input parameters: FWHM(Hβ), FWHM([OIII]), the equivalent widths of Hβ, [OIII], and FeII, [OIII]/Hβ and FeII/Hβ flux ratios, α_X, rest-frame 0.2-2.0 X-ray luminosity L_X, and the X-ray variability parameter χ^2/ν. The results of the PCA are summarized in Table 2. The first three Principal Components or Eigenvectors (EVs) account for more than 2/3 of the intrinsic variation in the data, or in other words, with the first three Eigen-

vectors, the data are already well-described. The most important Principal Component, Eigenvector 1, accounts for 32% of the variance. It clearly shows anti-correlations between the FWHM(Hβ) and FWHM([OIII]) and, as in the Boroson & Green (1992) Eigenvector 1 relationship, between [OIII]/Hβ and FeII/Hβ. When Eigenvector 1 increases, the X-ray spectra become steeper, the FeII/Hβ ratio increases and the [OIII] lines broadens while [OIII]/Hβ and FWHM(Hβ) decrease.

Figure 11 displays Eigenvector 1 vs. Eigenvector 2 and Eigenvector 3. The EV-1 vs. EV-2 diagram (left panel) shows that NLS1s and BLS1s lie basically in two different regions, with NLS1s having larger EV-1 values and lower EV-2 values than the BLS1s. There are a few BLS1s that fall in the NLS1s regime and vice-versa.

Figure 12 shows the correlation between Eigenvector 1 and the Eddington ratio $L/L_{\rm Edd}$ (left panel) and Eigenvector 2 with the black hole mass $M_{\rm BH}$ (right panel). Table 3 summarizes the Spearman rank order correlation coefficients and Student's t-test $t_{\rm S}$ values of the first two Eigenvectors with the black hole mass $M_{\rm BH}$, the rest-frame 0.2-2.0 keV X-ray luminosity $L_{\rm X}$ and the Eddington ratio $L/L_{\rm Edd}$. Clearly, EV-1 correlates with $L/L_{\rm Edd}$ and Eigenvector 2 with $M_{\rm BH}$ and $L_{\rm X}$. On the other hand, EV-1 only shows a marginal correlation with $M_{\rm BH}$ and EV-2 does not show any correlation with $L/L_{\rm Edd}$.

The correlations of Eigenvector 1 with $\alpha_{\rm X}$ and the Eddington ratio $L/L_{\rm Edd}$ suggest that also $\alpha_{\rm X}$ correlates with $L/L_{\rm Edd}$. As shown in the left panel of Figure 13 this is indeed the case. The correlation is strong with $r_{\rm S}$=+0.54 and $t_{\rm S}$=+6.71.

Eigenvector 2 shows an anti-correlation between X-ray luminosity and variability χ^2/ν and displays the same relationship as shown in § 3.1.8 and Figure 10. Eigenvector 2 itself is anti-correlated with the X-ray variability χ^2/ν and correlated with the luminosity and the FWHM(Hβ). This suggests that also χ^2/ν anti-correlates to the mass of the central black hole as it has been most recently reported by Papadakis (2004). The right panel in Figure 13 displays this anti-correlation with $r_{\rm S}$=–0.39 and $t_{\rm S}$=–4.33. Note that Papadakis (2004) used the excess variance (e.g. Nandra et al. (1997); George et al. (2000); Leighly (1999)) to describe the X-ray variability.

4. Discussion

4.1. Correlation Analysis

The sample presented here confirms the well-known FWHM(Hβ)-$\alpha_{\rm X}$ relationship among AGN (e.g. Boller et al. (1996); Grupe (1996); Laor et al. (1994, 1997); Grupe et al. (1999b); Vaughan et al. (2001)). Only NLS1s show very steep X-ray spectra while BLS1s never do. Also this sample confirms the findings of Grupe et al. (1999b) and Vaughan et al. (2001) that the FWHM(Hβ)-$\alpha_{\rm X}$ relationship is more pronounced among high-luminosity AGN. Interestingly, this relationship is also true for BLS1s samples (e.g. Xu et al. (2003)). The PCA of the soft X-ray selected sample shows that EV-1 can be interpreted as the Eddington ratio $L/L_{\rm Edd}$ and EV-2 possibly by the black hole mass $M_{\rm BH}$(see § 3.2 and § 4.2). Because a high $L/L_{\rm Edd}$ results in a steep X-ray spectrum (e.g. Pounds et al. (1995)) and a large $M_{\rm BH}$ results in a large FWHM(Hβ) (e.g. Kaspi et al. (2000); Peterson et al. (2000)) the FWHM(Hβ)-$\alpha_{\rm X}$ diagram is some what similar to the EV-1 EV-2 diagram (Figure 11a). This explains the 'zone of avoidance' in the FWHM(Hβ)-$\alpha_{\rm X}$ diagram: sources with broad Hβ lines and therefore large $M_{\rm BH}$ would require a mass accretion rate of about 10 $M_\odot$ yr^{-1} to reach their Eddington limit and display a steep X-ray spectrum. Even though this might be possible for a short time, e.g. during an X-ray outburst (e.g. Gezari et al. (2003)), it is very unlikely to find a BLS1 in that high outburst state over a long period of time.

Because FWHM(Hβ) $\propto$ $M_{\rm BH}$ (e.g. Peterson et al. (2000); Kaspi et al. (2000)) and FWHM([OIII])$\propto$ σ_* (Nelson (2000); Shields et al. (2003)) and the well-known $M_{\rm BH}$ – σ_* relationship between the central black hole mass and the bulge stellar velocity dispersion σ_* (e.g. Magorrian et al. (1998); Gebhardt et al. (2000); Tremaine et al. (2003)) one would expect to find a correlation between FWHM(Hβ) and FWHM([OIII]). Surprisingly, the Spearman rank order coefficient $r_{\rm S}$=+0.00 with $t_{\rm S}$=+0.01 between FWHM(Hβ) and FWHM([OIII]) does not confirm this assumption. In a separate paper (Grupe & Mathur (2004)) we will show that the $M_{\rm BH}$ – σ_* relationship does not apply for NLS1s, a result confirming the suggestions of Mathur et al. (2001), Wandel (2002), and Bian & Zhao

(2003).

The strongest (anti-)correlation among independent parameters of the soft X-ray selected AGN sample is the relation between FWHM(Hβ) and FeII/Hβ (§ 3.1.3). This strong relation suggests that strong FeII emission occurs in sources with high $L/L_{\rm Edd}$ and strong outflows, as we will discuss in the following section.

4.2. What do the Eigenvectors mean?

The crucial question of a PCA is whether the Eigenvectors have a physical interpretation. At first, one has to keep in mind, that there is not one 'Eigenvector 1' for every AGN sample. Each individual sample has its own PCA and therefore its own Eigenvectors. An Eigenvector always is specific to a certain sample depending on which observed parameters have been used and the range of the parameters. The Boroson & Green (1992) Eigenvector 1 (meaning the anti-correlation between the FeII and [OIII] strengths) does not has to be Eigenvector 1 for all samples. As an example, in the spectral PCA by Shang et al. (2003) Eigenvector 1 is the Baldwin effect and the Boroson & Green (1992) Eigenvector 1 turns out to be Eigenvector 3 in their PG quasar sample. However, PCAs are comparable to the Boroson & Green (1992) PCA if the input parameters and the ranges of the parameters used are similar to those of Boroson & Green (1992).

Nevertheless, the EV-1 of the PCA of the soft X-ray selected AGN sample is very similar to the Boroson & Green (1992) EV-1. Boroson (2002) and Sulentic et al. (2000) suggested that for their samples EV-1 can be interpreted as the Eddington ratio $L/L_{\rm Edd}$. The second Eigenvector EV-2 in the interpretation of Boroson (2002) would be the mass accretion rate $\dot{M}$. In this picture, NLS1 are sources with high Eddington ratio and low mass accretion rate $\dot{M}$. The present soft X-ray selected AGN sample seems to confirm these suggestions. As shown in Table 3, EV-1 strongly correlates with the Eddington ratio $L/L_{\rm Edd}$ and EV-2 with the X-ray luminosity $L_{\rm X}$ and therefore with the mass accretion rate $\dot{M}$ ($L = \eta * \dot{M} * c^2$). However, our EV-2 also strongly correlates with the mass of the black hole. The black hole masses for the soft X-ray selected sample were estimated by the relationships of Kaspi et al. (2000). It has become a popular idea that NLS1s have smaller black hole masses than BLS1s (e.g. Boller et al. (1996); Wandel & Boller (1998)). Also for this soft X-ray selected AGN sample I can confirm this suggestion (Grupe & Mathur (2004)). As shown in Grupe et al. (2004), in our sample the luminosity distributions of NLS1s and BLS1s are similar. In order for an object, like NLS1, with high Eddington ratios to show similar luminosities as objects with lower Eddington ratios is that their black hole masses are smaller for a given luminosity than those of BLS1s. However, this does not mean that individual NLS1s do not have large $M_{\rm BH}$. As a result of the high Eddington ratio, NLS1 are also the sources with the steepest X-ray spectra, as suggested by e.g. Pounds et al. (1995) and shown is Figure 13. It is also interesting to note that NLS1s seem to host preferentially in bared spiral galaxies (Crenshaw et al. 2003) which supposed to have better fueling rates than normal spirals and would support the result that NLS1s are the sources with the highest $L/L_{\rm Edd}$. The correlation between $\alpha_{\rm X}$ and $L/L_{\rm Edd}$ also explains the strong dependence of $L_{\rm X}$ on $\alpha_{\rm X}$ in NLS1s (Fig. 7). The Luminosities of NLS1s are governed by their Eddington ratio while in BLS1s their are governed by the mass of the central black hole.

A high Eddington ratio not only produces steep X-ray spectra it would also cause an outflow from the central region (e.g. Laor (2003) and references therein). King & Pounds (2003) showed recently that when the outflow rate $\dot{M}_{\rm out} \sim \dot{M}_{\rm Edd}$ the outflow will be optically thick and (at least in part) be responsible for the soft X-ray spectra seen in high accreting objects. Another consequence might be that the outflow affects the NLR and causes a radial velocity stratification with distance from the center (e.g. Laor (2003); Smith (1993)). This may explain the increase of the FWHM([OIII]) with increasing Eigenvector 1.

Strong outflows may also be responsible for the strong (anti-)correlation between FWHM(Hβ) and the FeII strength (§ 3.1.3). Strong optical FeII emission does not only occur in NLS1s, it also is strong in many Broad Absorption Line Quasars (BAL QSOs), well-known for their strong outflows (e.g. Yuan & Wills (2003); Hall et al. (2002); Weymann et al. (1991); Boroson & Meyers (1992)). Because strong FeII emission cannot be explained by simple photoionization models, Colin & Joly (2000) suggested that the strong

FeII emission found in NLS1s results from shocks which occur in outflows. This result also explain the correlation between the X-ray spectral index $\alpha_{\rm X}$ and FeII: sources with strong outflows have steep X-ray spectra and strong FeII emission.

As discussed by Boroson & Green (1992) the often-used orientation effect of Unified Schemes of AGN (e.g. Antonucci (1993); Urry & Padovani (1995)) does not explain Eigenvector 1 because the strength of the [OIII] emission should be independent of orientation if the NLR is isotropic. This assumption was confirmed for radio-quiet AGN by the findings of Kuraszkiewicz et al. (2000) who measured the [OII] and [OIII] emission in a sample of 20 PG quasars and found that EV-1 correlates with the orientation-independent [OII] and [OIII] emission. As shown in Table 2 also the PCA of the soft X-ray AGN sample shows correlations between EV-1 and [OIII]/Hβ and EW([OIII]) suggesting that EV-1 is not an orientation effect. One alternative explanation of Eigenvector 1 was mentioned by Brandt & Boller (1999) who suggested that it could be the rotation of the black hole and NLS1 should be sources with slowly spinning black holes. This was based on the findings of Boroson & Green (1992) that objects with a large radio loudness have weaker FeII and stronger [OIII] emission. The driver for radio-loudness is thought to be the spinning of the black hole (e.g. Wilson & Colbert (1995)). However, as Boroson & Green (1992) also remarked, a slowly spinning black hole would not explain the properties of ultrasoft NLS1s. Another argument against this assumption is that meanwhile a number of radio-loud NLS1 have been found (e.g. Remillard et al. (1991); Siebert et al. (1999); Grupe et al. (2000)) which do not fit into this picture. It has also been shown by e.g. Laor (2000) and Lacy et al. (2001) that there is a correlation between the radio loudness and $M_{\rm BH}$. Because the correlation between EV-1 and $M_{\rm BH}$ is found to be marginal (Table 3) a link between EV-1 and the radio loudness is unlikely for the soft X-ray selected AGN sample.

As shown in Table 3 there are two most likely interpretation of Eigenvector 2: the black hole mass $M_{\rm BH}$ and the mass accretion rate $\dot{M}$ as suggested by Boroson (2002). For both properties, EV-2 shows strong correlations. Arguing for the black hole mass $M_{\rm BH}$ as the interpretation of EV-2 is the correlation with the FWHM(Hβ) (Table 2). This together with the correlation with luminosity and the relationships of Kaspi et al. (2000) to determine $M_{\rm BH}$ makes the black hole mass a plausible explanation of EV-2. However, this does not necessarily explain the strong weight of the X-ray variability parameter χ^2/ν in EV-2. On the first view, the X-ray variability argues more for the mass accretion rate as the interpretation of EV-2. If the mass accretion rate is low, a small change in the mass accretion rate results in a higher variability than for objects with high mass accretion rates. On the other hand, recently Papadakis (2004) reported of a correlation between X-ray variability and the mass of the central black hole in a sample of 14 AGN supporting the suggestion that EV-2 represents the black hole mass. With the current set of parameters to study the soft X-ray sample it is not possible to give a final interpretation of EV-2, whether it is $M_{\rm BH}$ or $\dot{M}$.

The difference between the PCA of the soft X-ray selected AGN sample and the PG quasar sample of Boroson (2002) is that his EV-1 is strongly correlated with $M_{\rm BH}$ (Table 2 in Boroson (2002)) which is not the case for the soft X-ray AGN sample (Table 3). Because in the Boroson (2002) sample EV-1 as well as EV-2 are correlated with $M_{\rm BH}$ the mass accretion rate $\dot{M}$ is more likely the explanation for EV-2 than $M_{\rm BH}$. However, the slight correlation of EV-1 with $L_{\rm X}$ (and therefore $\dot{M}$) in the PCA of the soft X-ray AGN sample and the weak correlation between EV-1 and $M_{\rm BH}$ makes the black hole mass $M_{\rm BH}$ a more plausible interpretation of our EV-2 than $\dot{M}$.

4.3. Are NLS1 young AGN?

The Eddington ratio $L/L_{\rm Edd}$ (and therefore EV-1) can be interpreted as the 'age' of an AGN. In early phases of the AGN development the accretion rate would be close to the Eddington limit and decreases at later phases. In this picture NLS1 would be AGN in an early phase of the AGN development (Grupe (1996); Grupe et al. (1999b); Mathur (2000)). One has to be careful with the term 'age'. Eigenvector 1 or $L/L_{\rm Edd}$ do not measure an age in terms of years, it is more how early in the evolution of the AGN we see the source, like e.g. T-Tauri stars are stars in an early state of the stellar evolution while red giants are in a later state. A high Eddington ratio in the early phase of the AGN development would not only produce

steep X-ray spectra (e.g. Pounds et al. (1995)) it would also result in strong mass outflows (e.g. King & Pounds (2003). There is growing evidence at optical/UV and X-ray energies for such strong outflows in NLS1s (e.g. Goodrich (2000); Grupe et al. (2001b); Leighly et al. (1997); Zamanov et al. (2002); Sako et al. (2001); Kaspi et al. (2002); Behar et al. (2003); Pounds et al. (2003)).

Mathur (2000) suggested that NLS1 are low-redshift cousins of high-redshift QSOs and both are AGN in an early state of their evolution. This assumption recently got observational support by the findings of Yuan & Wills (2003) from rest-frame optical spectra of high-redshift QSOs. They found that a) high-redshift QSOs are high accreting sources just like NLS1 and b) they follow the Boroson & Green Eigenvector 1 relationship. On the other hand, Constantin & Shields (2003) argued on the basis of UV spectroscopy of NLS1 and high-redshift QSOs that they are not. However, Constantin & Shields (2003) used UV line parameters and performed a spectral PCA using the UV data of NLS1 and high-redshift quasars. These are different input parameters than in the Boroson & Green Eigenvector 1, like Yuan & Wills (2003) did for their sample.

The reason why about 50% of the objects in the soft X-ray AGN sample are NLS1 is simply a selection effect: the objects of the sample were selected by being X-ray soft and NLS1s are the sources with the softest X-ray spectra. One crucial point in the interpretation of NLS1 is what their black hole mass really is. For the sample presented here the black hole masses were derived from the relationship given in Kaspi et al. (2000). This assumes that the radius of the BLR of NLS1 scales with luminosity in the same way as for BLS1s. This issue will be discussed in a separate paper (Grupe & Mathur (2004)).

One of the most fundamental relation found in nearby galaxies and AGN is the black hole mass to bulge stellar velocity dispersion $M_{\rm BH} - \sigma_*$ relation that links properties of the central black hole with the host galaxy (e.g. Magorrian et al. (1998) and Tremaine et al. (2003)). However, NLS1s seem to deviate from this relation as shown by e.g. Mathur et al. (2001); Wandel (2002); Zheng et al. (2002) and Grupe & Mathur (2004). As shown by Grupe & Mathur (2004) those objects deviate from the Tremaine et al. (2003) relation that have the highest $L/L_{\rm Edd}$ namely NLS1s. On the other hand these are the sources with the smallest black hole masses. The interpretation is that NLS1s are young objects in which the black hole is still growing and evolving towards the Tremaine et al. (2003) $M_{\rm BH} - \sigma$ relation (Grupe & Mathur 2004).

4.4. Classification of the Seyfert types

In Paper I and in this paper we/I adopted the standard definition of Goodrich (1989) to separate NLS1s and BLS1s. However, even though this is an easy method, it fails for a number of sources which have FWHM(Hβ) >2000 km s^{-1}and are therefore classified as BLS1s, but show all characteristics as NLS1s such as strong FeII emission, weak [OIII] and steep X-ray spectra and therefore a high EV-1 which puts them into the region of NLS1s (Figure 11). Namely these sources are RX J1005.7+4332 and IRAS 1334+2438. There are also two NLS1s which happen to lie in the BLS1s region: Mkn 110 and PKS 2227–299, which can also be classified as Seyfert 1.5s and form a separate subclass. Future classification should take the X-ray and optical properties of NLS1s into account to separate between different Seyfert groups. Even though every separation between these types are arbitrary because of the continuous properties of the sources, the classification just on the basis of the FWHM(Hβ) is not enough to describe the classes properly.

5. Conclusions

I have presented a statistical analysis of a complete sample of 110 soft X-ray selected AGN and found:

- The objects in this sample follow the Boroson & Green Eigenvector 1 which can be most likely interpreted as the Eddington ratio $L/L_{\rm Edd}$.
- Eigenvector 2 of the soft X-ray selected sample is most likely the black hole mass $M_{\rm BH}$.
- The Eddington ratio $L/L_{\rm Edd}$ and therefore Eigenvector 1 can be interpreted as the 'age' of the AGN.

- NLS1 in this picture are AGN with a high $L/L_{\rm Edd}$ in a young phase of their evolution.
- The soft X-ray AGN sample follows the well-known FWHM$H(\beta)$-$\alpha_{\rm X}$ relationship
- The FeII strength strongly anti-correlates with FWHM(Hβ) and correlates with $\alpha_{\rm X}$.
- The soft X-ray spectral index $\alpha_{\rm X}$ correlates with $L/L_{\rm Edd}$ and the X-ray variability parameter χ^2/ν anti-correlates with $M_{\rm BH}$.

The sample presented here is complete with respect to the selection criteria given in the introduction. Therefore, absorbed, faint and higher-redshift objects are excluded. Future studies of the sample will be to extend the sample towards these sources in order to improve the statistical significance of the correlations.

I would like to thank Bev Wills, Karen Leighly, Stefanie Komossa and Marianne Vestergaard for discussions and comments on this paper, and the anonymous referee for his/her suggestions on the manuscript to improve the final paper. This research has made use of the NASA/IPAC Extragalactic Database (NED) which is operated by the Jet Propulsion Laboratory, Caltech, under contract with the National Aeronautics and Space Administration. The ROSAT project is supported by the Bundesministerium für Bildung und Forschung (BMBF/DLR) and the Max-Planck-Society.

REFERENCES

Antonucci, R.R.J., 1999, ARA&A, 31, 473

Barr, P., & Mushotzky, R.F., 1986, Nature, 330, 421

Beuermann, K., Thomas, H.-C., Reinsch, K., et al., 1999, A&A, 347, 47

Becker, R.H., White, R.L., Gregg, M.D., Brotherton, M.S., Laurent-Muehleisen, S.A., & Arav, N., 2000, ApJ, 538, 72

Behar, E., Rasmussen, A.P., Blustin, A.J., Sako, M., Kahn, S.M., Kaastra, J.S., Branduardi-Raymond, G., & Steenbrugge, K.C., 2003, ApJ, in press (astro-ph/0307467)

Bian, W., & Zhao, Y., 2003, MNRAS in press, astro-ph/0309701

Boller, T., Brandt, W.N., & Fink, H.H., 1996, A&A, 305, 53

Boroson, T.A., 2002, ApJ, 565, 78

Boroson, T.A., & Green, R.F., 1992, ApJS, 80, 109

Boroson, T.A., & Meyers, K.A., 1992, ApJ, 397, 442

Brandt, W.N., Pounds, K.A., & Fink, H.H., 1995, MNRAS, 273, L47

Brandt, W.N., Mathur, S., & Elvis, M., 1997, MNRAS, 285, L25

Brandt, W.N., & Boller, T., 1999, ASP Conf. Series Vol. 175, 'Structure and Kinematics of Quasar Broad Line Regions' eds C.M. Gaskell, W.N. Brandt, M. Dietrich, D. Dultzin-Hacyan & M. Eracleous, p265

Brinkmann, W., Grupe, D., Branduardi-Raymond, G., & Ferrero, E., 2003, A&A, 398, 81

Colin, S., & Joly, M., 2000, New Astronomy Reviews Vol. 44, proceedings of the workshop on 'Observational and Theoretical Progress in the Study of Narrow-Line Seyfert 1 Galaxies, Eds Th. Boller, W.N. Brandt, K.M. Leighly, and M.J. Ward, p531

Constantin, A., & Shields, J.C., 2003, PASP, 115, 592

Crenshaw, D.M., Kraemer, S.B., & Gabel, J.R., 2003, AJ, 126, 1690

Dickey, J.M., & Lockman, F.J., 1990, ARA&A, 28, 215

Edelson, R., Vaughan, S., Warwick, R., Puchnarewicz, E., & George, I., 1999, MNRAS, 307, 91

Elvis, M., Fiore, F., Wilkes, B.J., & McDowell, J., 1994, ApJ, 422, 60

Francis, P.J., & Wills, B.J., 1999, ASP Conf. Series 162, p163

Gebhardt, K., Bender, R., Bower, G., Dressler, A., Faber, S.M., et al., 2000, A&A, 539, L13

George, I.M., Turner, T.J., Yaqoob, T., Netzer, H., Laor, A., Mushotzky, R.F., Nandra, K., Takahashi, T., 2000, ApJ, 531, 52

Gezari, S., Halpern, J.P., Komossa, S., Grupe, D., & Leighly, K.M., 2003, ApJ, 592, 42

Goodrich, R.W., 1989, ApJ, 342, 224

Goodrich, R.W., 2000, New Astr. Rev. vol. 44, p519

Green, A.R., McHardy, I.M., & Lehto, H.J., 1993, MNRAS, 265, 664

Grupe, D., 1996, PhD Thesis, Universität Göttingen

Grupe, D., 2000, New Astronomy Reviews Vol. 44, proceedings of the workshop on 'Observational and Theoretical Progress in the Study of Narrow-Line Seyfert 1 Galaxies, Eds Th. Boller, W.N. Brandt, K.M. Leighly, and M.J. Ward, p455

Grupe, D., Beuermann, K., Mannheim, K., et al., 1995a, A&A, 299, L5

Grupe, D., Beuermann, K., Mannheim, K., Thomas, H.-C., Fink, H.H., & de Martino, D., 1995b, A&A, 300, L21

Grupe, D., Beuermann, K., Thomas, H.-C., & Fink, H.H., 1998a, A&A, 330, 25

Grupe, D., Wills, B.J., Wills, D., Beuermann, K., 1998b, A&A, 333, 827

Grupe, D., Thomas, H.-C., & Leighly, K.M., 1999a, A&A, 350, L31

Grupe, D., Beuermann, K., Mannheim, K., & Thomas, H.-C., 1999, A&A, 350, 805

Grupe, D., Leighly, K.M., Thomas, H.-C., & Laurent-Muehleisen, S.A., A&A, 356, 11

Grupe, D., Thomas, H.-C., & Beuermann, K., 2001, A&A, 367, 470

Grupe, D., Thomas, H.-C., Leighly, K.M., 2001b, A&A, 369, 450

Grupe, D., Wills, B.J., Leighly, K.M., & Meusinger, H., 2004, AJ, in press, Paper I, astro-ph/0310027

Grupe, D., & Mathur, S., 2004, ApJL submitted

Hall, P.B., Anderson, S.F., Strauss, M.A., et al., 2002, ApJS, 141, 267

Kaspi, S., Smith, P.S., Netzer, H., Moaz, D., Jannuzi, B.T., & Giveon, U., 2000, ApJ, 533, 631

Kaspi, S., Brandt, W.N., George, I.M., et al. 2002, ApJ, 574, 643

King, A.R., & Pounds, K.A., 2003, MNRAS, in press, astro-ph/0305541

Kuraszkiewicz, J., Wilkes, B.J., Brandt, W.N., & Vestergaard, M., 2000, ApJ, 542, 631

Lacy, M., Laurent-Muehleisen, S.A., Ridgway, S.E., Becker, R.H., & White, R.L., 2001, ApJ, L17

Laor, A., Fiore, F., Elvis, M., Wilkes, B.J., & McDowell, J.C., 1994, ApJ, 435, 611

Laor, A., Fiore, F., Elvis, M., Wilkes, B.J., & McDowell, J.C., 1997, ApJ, 477, 93

Laor, A., 1998, ApJ, 505, L83

Laor, A., 2000, ApJ, 543, L111

Laor, A., 2003, ApJ, 590, 86

Laor, A., Fiore, F., Elvis, M., Wilkes, B.J., & McDowell, J.C., 1997, ApJ, 477, 93

Lawrence, A., & Papadakis, I., 1993, ApJ, 414, L85

Leighly, K.M., Mushotzky, R.F., Nandra, K., & Foster, K., 1997, ApJ, 489, L25

Leighly, K.M., 1999, ApJS, 125, 297

Magorrian, J., Tremaine, S., Richstone, D., Bender, R., Bower, G., et al., 1998, AJ, 115, 2285

Marziani, P., Sulentic, J.W., Dultzin-Hacyan, D., Calvani, M., & Moles, M., 1996, ApJS, 104, 37

Marziani, P., Sulentic, J.W., Calvani, M., Dultzin-Hacyan, D., Bachev, R., & Zwitter, T., 2003, ApJS, 147, 199

Mathur, S., 2000, MNRAS, 314, L17

Mathur, S., Kuraszkiewicz, J., & Czerny, B., 2001, New Astronomy, Vol. 6, p321

Nandra, K., George, I.M., Mushotzky, R.F., Turner, T.J., Yaqoob, T., 1997, ApJ, 476, 70

Nelson, C.H., 2000, ApJ, 544, L91

Osterbrock, D.E., & Pogge, R.W., 1985, ApJ, 297, 166

Papadakis, I.E., 2004, MNRAS, in press, astro-ph/0310016

Peterson, B.M., McHardy, I.M., Wilkes, B.J., Berlind, P., Bertram, R., et al., 2000, ApJ, 542, 161

Pfeffermann, E., Briel, U.G., Hippmann, H., et al., 1987, SPIE, 733, 519

Pounds, K.A., Done, C., & Osborne, J., 1995, MNRAS, 277, L5

Pounds, K.A., Reeves, J.N., King, A.R., Page, K.L., O'Brian, P.T., & Turner, M.J.L., 2003, MNRAS, in press (astro-ph/0303603)

Puchnarewicz, E.M., Mason, K.O., Córdova, F.A., et al., MNRAS, 256, 589

Rees, M.J., 1990, Science, 247, 817

Remillard, R.A., Grossan, B., Bradt, H.V., Ohashi, T., & Hayashida, K., 1991, Nat, 350, 589

Sako, M., Kahn, S.M., Behar, E., et al., 2001, A&A, 365, L168

Schwope, A.D., Hasinger, G., Lehmann, I., et al., AN, 321, 1

Shang, Z., Wills, B.J., Robinson, E.L., Wills, D., Laor, A., Xie, B., & Yuan, J., 2003, ApJ, 586, 52

Shields, G.A., 1978, Nature, 272, 706

Shields, G.A., Gebhardt, K., Salviander, S., Wills, B.J., Xie, B., Brotherton, M.S., Yuan, J., & Dietrich, M., 2003, ApJ, 583, 124

Siebert, J., Leighly, K.M., Laurent-Muehleisen, S.A., Brinkmann, W., Boller, T., & Matsuoka, M., 1999, A&A, 348, 678

Sigut, T.A.A., & Pradhan, A.K., 2003, ApJ, in press, astro-ph/0206096

Smith, S.J., 1993, ApJ, 411, 570

Stepanian, J.A., Benítez, E., Krongold, Y., et al., 2003, ApJ, 588, 746

Stephens, S., 1989, AJ, 97, 10

Sulentic, J.W., Zwitter, T., Marziani, P., & Dultzin-Hacyan, D., 2000, ApJ, 536, L5

Sulentic, J.W., Marziani, P., Zamanov, R., Bachev, R., Calvani, M., Dultzin-Hacyan, D., 2002, ApJ, 566, L71

Thomas, H.-C., Beuermann, K., Reinsch, K., et al., 1998, A&A, 335, 467

Tremaine, S., Gebhardt, K., Bender, R., et al., 2003, ApJ, 574, 740

Turner, T.J., George, I.M., Grupe, D., et al., 1999, ApJ, 510, 178

Vaughan, S., Edelson, R., Warwick, R.S., Malkan, M,A., & Goad, M.R., 2001, MNRAS, 327, 673

Veilleux, S & Osterbrock, D.E., 1987, ApJS, 63, 295

Urry, M.C., & Padovani, P., 1995, PASP, 107, 803

Voges, W., Aschenbach, B., Boller, T., et al., 1999, A&A, 349, 389

Wandel, A., & Boller, T., 1998, A&A, 331, 884

Wandel, A., 2002, ApJ, 565, 762

Weymann, R.J., Morris, S.L., Foltz, C.B., Hewett, P.C., 1991, ApJ, 373, 21

Wilkes, B.J., Elvis, M., & McHardy, I., 1987, ApJ, 321, L23

Williams, R.J., Pogge, R.W., & Mathur, S., 2003, AJ, 124, 3042

Williams, R.J., Pogge, R.W., & Mathur, S., 2004, AJ, in preparation

Wills, B.J., Wills, D., Evans, N.J., Natta, A., Thompson, K.L., Breger, M., & Sitko, M.L., 1992, ApJ, 400, 96

Wilson, A.S., & Colbert, E.J., 1995, ApJ, 438, 62

Xu, D.W., Komossa, S., Wei, J.Y., Qian, Y, & Zheng, X.Z., 2003, ApJ, 590, 73

York D.G., et al., 2000, AJ, 120, 1579

Yuan, M.J., & Wills, B.J., 2003, ApJ, 593, L11

Zamanov, R., Marzini, P., Sulentic, J.W., Calvani, M., Dultzin-Hacyan, D., & Bachev, R., 2002, ApJ, 576, L9

Zheng, X.Z., Xia, X.Y., Mao, S., Wu, H., & Deng, Z.G., 2002, AJ, 124, 18

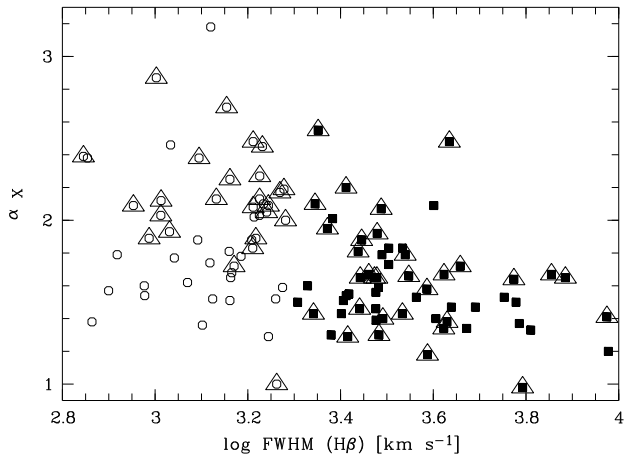

Fig. 1.— log FWHM(Hβ) vs. X-ray spectral slope $\alpha_{\rm X}$; NLS1 are coded as open circles and BLS1s and filled squares. In addition, high-luminous AGN (log $L_{\rm X}$ >37.0 [W]) are displayed as triangles that surround the circles and squares.

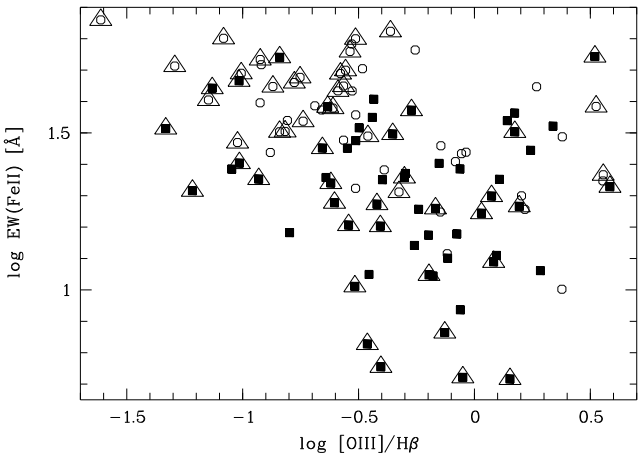

Fig. 3.— log [OIII]/Hβ flux ratio vs. log EW(FeII); Symbols are as described in Figure 1.

This 2-column preprint was prepared with the AAS LaTeX macros v5.2.

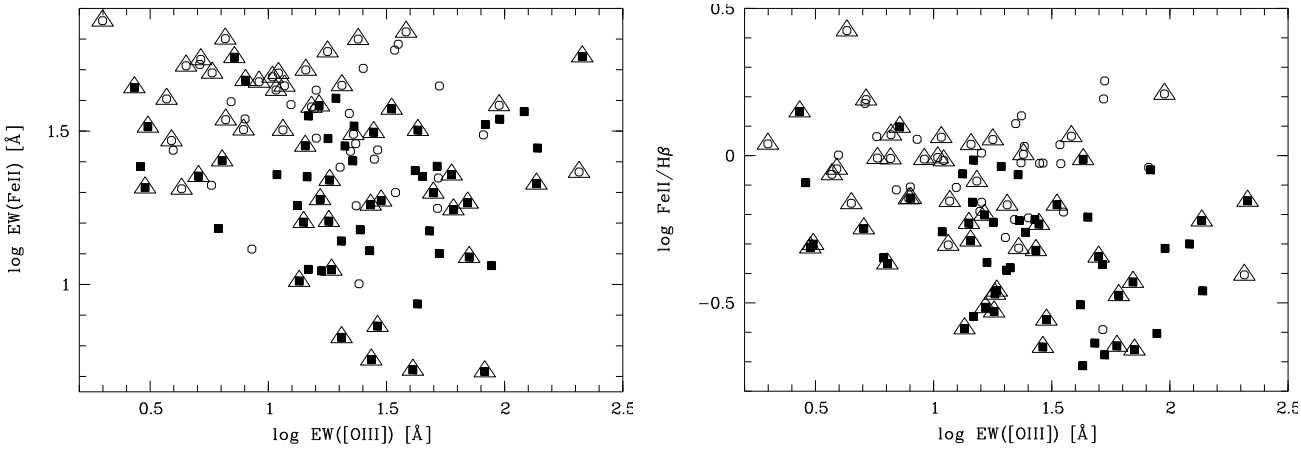

Fig. 2.— log EW([OIII]) vs. log EW(FeII) (left) and log FeII/Hβ (right), X-ray spectral slope $\alpha_{\rm X}$; Symbols are as described in Figure 1.

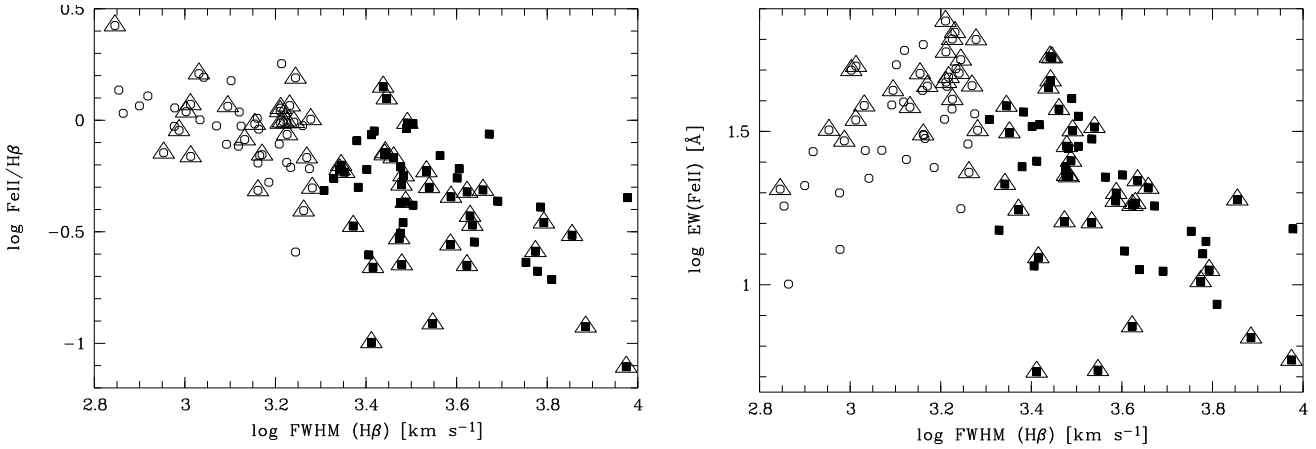

Fig. 4.— log FWHM(Hβ) vs. log FeII/Hβ (left) and EW(FeII) (right); Symbols are as described in Figure 1.

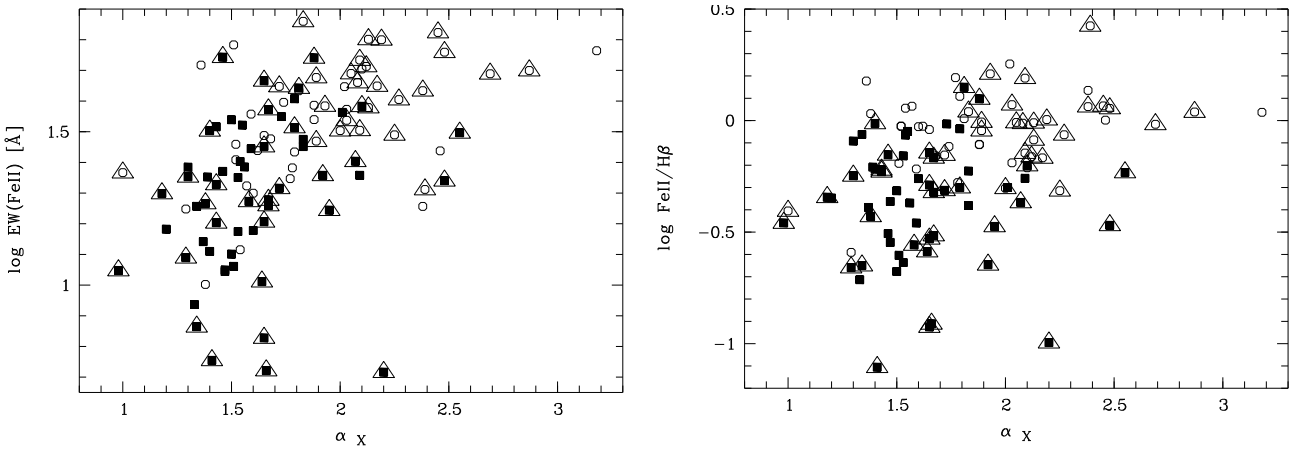

Fig. 5.— X-ray spectral slope α_X vs. log EW(FeII) (left) and log FeII/Hβ (right); Symbols are as described in Figure 1.

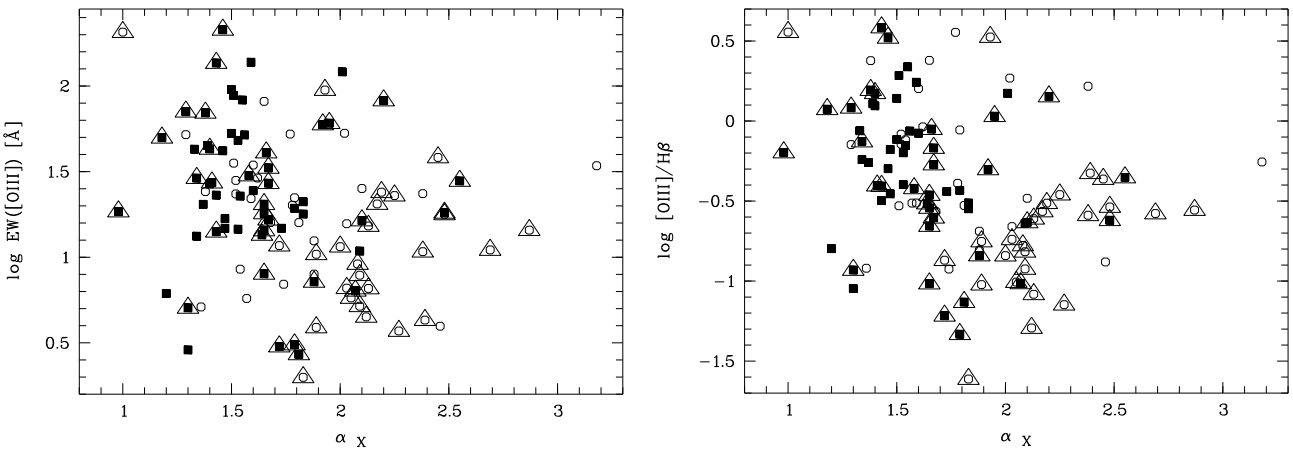

Fig. 6.— X-ray spectral slope α_X vs. log EW([OIII]) (left) and log [OIII]/Hβ flux ratio (right). Symbols are as described in Figure 1.

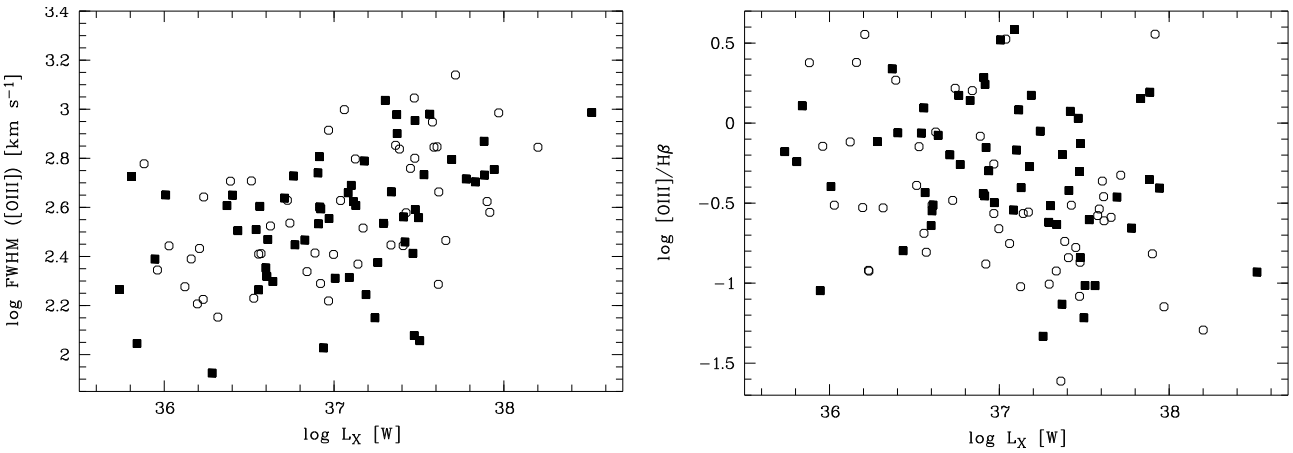

Fig. 8.— Soft X-ray luminosity log $L_{\rm X}$ vs. log FWHM([OIII]) (left) and log [OIII]/Hβ flux ratio (right). Symbols are as described in Figure 1.

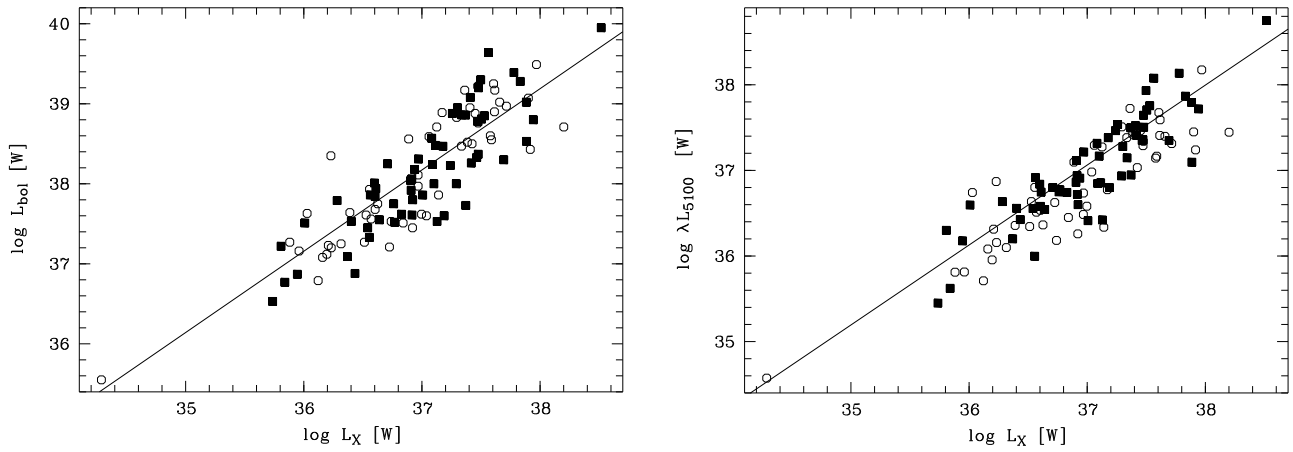

Fig. 9.— Rest-frame 0.2-2.0 X-ray luminosity $L_{\rm X}$ vs. bolometric luminosity $L_{\rm bol}$ (left) and monochromatic luminosity at (rest-frame) 5100Å $\lambda L_{5100\mathring{\rm A}}$ (right). The solid lines are the regression curves given in Eqs. 1 and 2 in § 3.1.7. Symbols are as described in Figure 1.

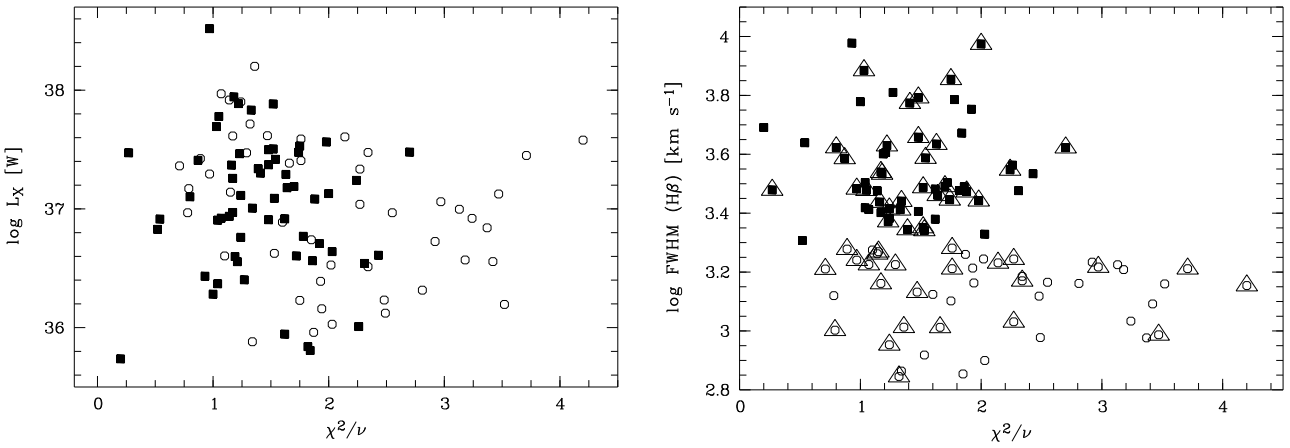

Fig. 10.— Soft X-ray variability parameter χ^2/ν vs. rest-frame 0.2-2.0 X-ray luminosity $L_{\rm X}$ and FWHM(Hβ). NGC 4051, Mkn 766, and RX J1304.2+0205 are of the plots (χ^2/ν=18.5, 8.86, and 5.08, respectively). Symbols are as described in Figure 1.

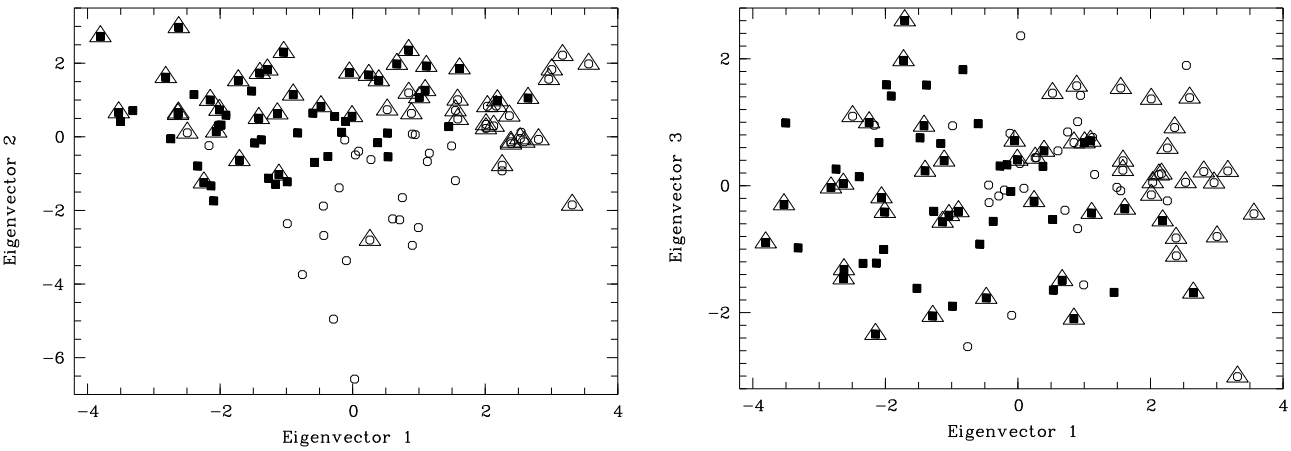

Fig. 11.— Eigenvector 1 vs. Eigenvector 2 (left) and Eigenvector 3 (right) of the Soft X-ray selected AGN sample. Symbols are as described in Figure 1.

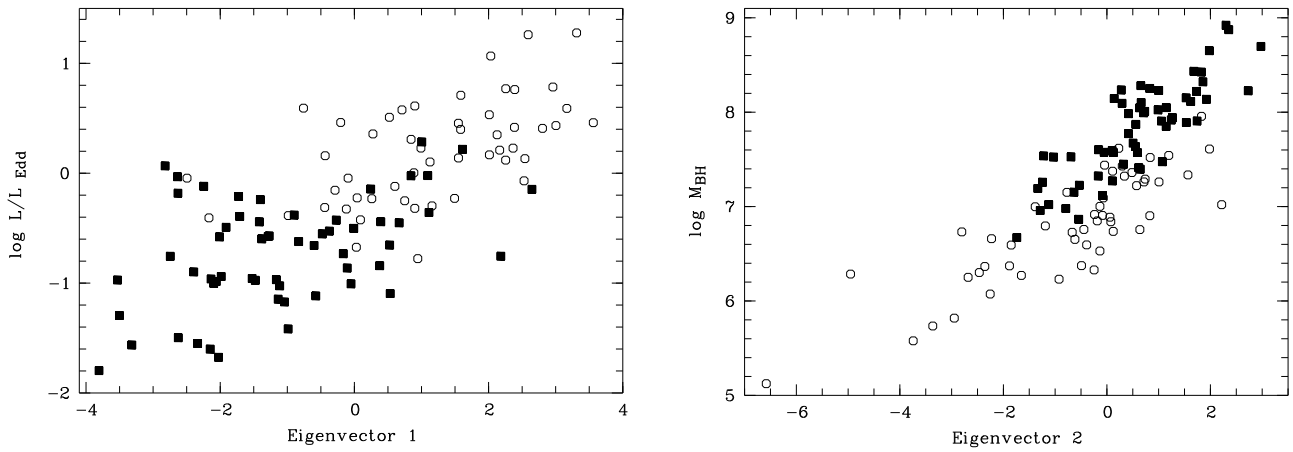

Fig. 12.— Eigenvector 1 vs. Eddington ratio $L/L_{\rm Edd}$ (left) and Eigenvector 2 (right) vs. black hole mass (right) given in units of $M_{\odot}$. Symbols are as described in Figure 1.

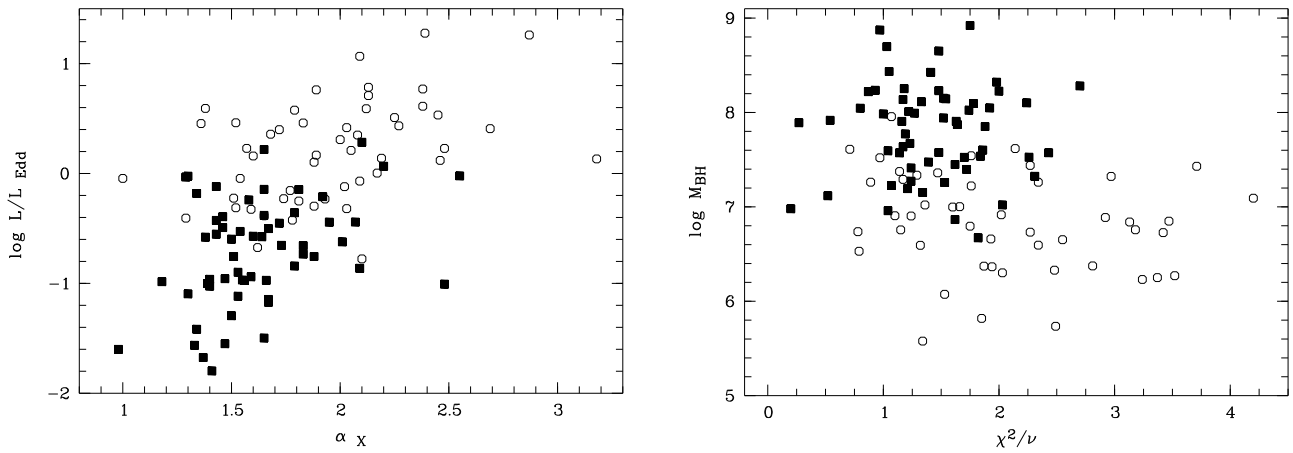

Fig. 13.— X-ray spectral index $\alpha_{\rm X}$ vs. Eddington ratio $L/L_{\rm Edd}$ (left) and χ^2/ν vs. black hole mass (right) given in units of $M_{\odot}$. Symbols are as described in Figure 1.

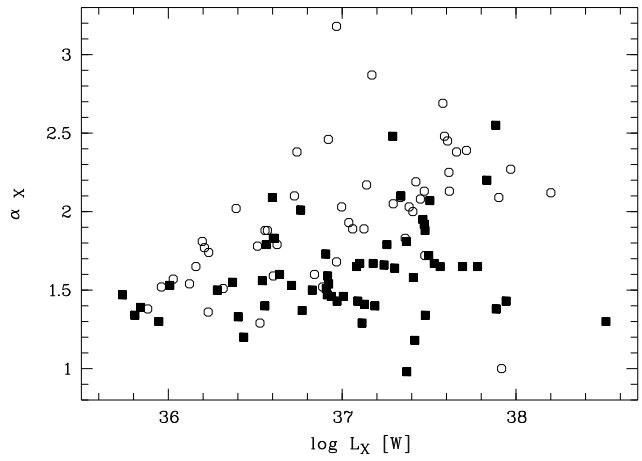

Fig. 7.— Soft X-ray rest-frame 0.2-2.0 X-ray luminosity vs. $\alpha_{\rm X}$. Symbols are as described in Figure 1.

TABLE 1

SPEARMAN RANK ORDER CORRELATION (BELOW DIAGONAL) AND STUDENT'S T-TEST FOR THE SIGNIFICANCE OF THE CORRELATION (ABOVE DIAGONAL).

	FWHM Hβ	FWHM [OIII]	EW Hβ	EW [OIII]	EW FeII	[OIII]/Hβ	FeII/Hβ	α_X	$logL_X$	χ^2/ν
	all	+0.01	+2.02	+1.88	**−5.84**	+0.92	**−10.5**	**−5.34**	+0.61	**−3.99**
	high L_X	*−1.30*	*+0.47*	*+2.31*	**−6.05**	*+1.95*	**−7.50**	**−6.01**	*−0.79*	*−0.97*
FWHM(Hβ)	low L_X	+0.67	+2.40	+0.63	−2.46	−0.38	**−7.50**	**−3.18**	+0.38	**−4.30**
	NLS1s	*−0.28*	**+5.72**	*+1.10*	**+3.30**	*−1.27*	**+3.34**	*−0.01*	*+1.26*	*−1.27*
	BLS1s	+0.57	−1.00	−2.23	**−4.88**	−1.55	**−3.35**	−2.10	−0.44	−0.00
	+0.00	all	+0.23	−2.79	+1.80	−2.42	+1.66	+2.54	**+5.41**	−1.21
	−0.17	high L_X	*−1.32*	**−3.45**	*+1.40*	*−2.42*	*+2.49*	*+0.62*	*+2.47*	*+0.67*
FWHM([OIII])	+0.09	low L_X	−0.13	+0.59	+0.33	+1.53	+0.50	+1.20	+0.90	−1.37
	−0.04	NLS1s	*+0.57*	*−1.80*	*−1.63*	*−0.35*	*+1.72*	**+3.70**	**+4.26**	*−1.66*
	+0.08	BLS1s	−0.40	−2.41	+0.38	−2.21	+0.72	+0.75	**+3.51**	−0.24
	+0.19	+0.02	all	+0.33	**3.65**	**−3.46**	**−4.88**	+2.14	**+3.30**	−2.19
	+0.06	*−0.18*	high L_X	*+0.23*	*+1.77*	*−2.03*	*−1.98*	*+0.79*	*−0.30*	*−1.84*
EW(Hβ)	+0.32	−0.02	low L_X	+1.97	**+3.35**	−2.25	**−5.60**	+0.60	**+3.02**	−0.70
	+0.63	*+0.08*	NLS1s	*−0.47*	**+5.35**	**−3.88**	**−5.84**	*+0.88*	*+2.87*	*−2.01*
	−0.13	−0.05	BLS1s	+2.11	+2.21	−1.06	−2.92	**3.59**	+1.59	−0.11
	+0.18	−0.26	+0.10	all	−2.98	**+19.6**	**−4.11**	**−3.34**	−2.04	−0.72
	+0.30	**−0.42**	*+0.03*	high L_X	**−3.07**	**+17.5**	**−3.89**	*−2.34*	*−1.51*	*−0.07*
EW([OIII])	+0.09	+0.08	+0.27	low L_X	−0.37	**+9.61**	−2.09	−0.48	+0.98	−1.29
	+0.16	*−0.25*	*−0.07*	NLS1s	*−1.39*	**+11.0**	*−0.80*	*−1.90*	*−2.35*	*+0.43*
	−0.28	−0.30	+0.27	BLS1s	−0.81	**+15.1**	−2.58	−0.96	−0.89	−0.07
	−0.49	+0.17	**+0.33**	−0.28	all	**−5.23**	**+8.50**	**+6.87**	+1.6	+1.21
	−0.63	*+0.19*	*+0.26*	**−0.38**	high L_X	**−4.03**	**+10.7**	**+4.64**	*−0.19*	*+0.55*
EW(FeII)	−0.33	+0.05	**+0.42**	−0.05	low L_X	−2.61	+2.81	**+4.52**	+1.24	+1.77
	+0.43	*+0.29*	**+0.61**	*−0.19*	NLS1s	**−4.30**	*+0.59*	**+3.61**	*+2.88*	*−1.37*
	−0.54	+0.05	+0.28	−0.11	BLS1s	−1.74	**+8.52**	**+3.15**	+0.05	−0.06
	+0.09	−0.23	**−0.32**	**+0.88**	**−0.45**	all	−1.90	**−4.53**	**−3.60**	−0.24
	+0.25	−0.31	*−0.22*	**+0.92**	**−0.48**	high L_X	*−2.91*	*−2.58*	*1.20*	*+0.03*
[OIII]/Hβ	−0.05	+0.20	−0.30	**+0.80**	−0.34	low L_X	+0.29	−0.75	−0.67	−1.20
	−0.18	*−0.23*	**−0.49**	**+0.84**	**−0.53**	NLS1s	*+1.20*	*−2.18*	**−3.28**	*0.40*
	−0.20	−0.28	−0.14	**+0.89**	−0.22	BLS1s	−1.19	**−2.57**	−1.91	+0.15
	−0.71	+0.16	**−0.43**	**−0.37**	**+0.63**	−0.18	all	**+4.57**	−1.29	+2.97
	−0.71	+0.32	*−0.26*	**−0.46**	**+0.82**	**−0.37**	high L_X	**+4.15**	*−0.15*	*+1.29*
FeII/Hβ	**−0.72**	+0.07	**−0.62**	−0.28	+0.37	+0.04	low L_X	+2.79	−1.82	+2.50
	−0.42	*+0.24*	**−0.64**	*−0.11*	*+0.08*	*+0.17*	NLS1s	*+1.69*	*−0.68*	*+0.07*
	−0.40	+0.10	−0.36	−0.32	**+0.75**	−0.16	BLS1s	+0.47	−1.42	+0.38
	−0.46	+0.24	+0.20	**−0.31**	**+0.55**	**−0.40**	**+0.40**	all	**+4.22**	+1.17
	−0.63	*+0.08*	*+0.11*	*−0.30*	**+0.53**	*−0.33*	**+0.49**	high L_X	*+1.51*	*+0.49*
α_X	**−0.41**	+0.17	+0.08	−0.07	**+0.53**	−0.10	+0.36	low L_X	+2.29	**+3.20**
	−0.00	**+0.47**	*+0.13*	*−0.26*	**+0.46**	*−0.30*	*+0.23*	NLS1s	**+5.73**	−1.30
	−0.27	+0.10	**+0.43**	−0.13	**+0.39**	−0.32	+0.06	BLS1s	+1.96	+0.19
	+0.06	**+0.46**	**+0.30**	−0.19	+0.16	**−0.33**	−0.12	**+0.38**	all	−2.81
	−0.11	+0.32	*−0.04*	*−0.20*	*−0.03*	*−0.14*	*−0.02*	*+0.20*	high L_X	*−1.31*
log L_X	+0.05	+0.13	**+0.39**	+0.14	+0.17	−0.09	−0.25	+0.30	low L_X	−1.40
	+0.18	**+0.52**	*+0.38*	*−0.32*	*+0.38*	*−0.42*	*−0.10*	**+0.63**	NLS1s	*−2.68*
	−0.06	**+0.42**	+0.21	−0.12	+0.01	−0.25	−0.19	+0.25	BLS1s	−0.71
	−0.36	−0.12	−0.21	−0.07	+0.12	−0.02	+0.28	+0.11	−0.26	all
	−0.13	*+0.09*	*−0.24*	*−0.01*	*+0.07*	*+0.01*	*+0.17*	*+0.07*	*−0.17*	high L_X
χ^2/ν	**−0.51**	−0.19	−0.10	−0.17	+0.24	−0.18	+0.33	**+0.41**	−0.19	low L_X

TABLE 1—*Continued*

FWHM Hβ	FWHM [OIII]	EW Hβ	EW [OIII]	EW FeII	[OIII]/Hβ	FeII/Hβ	α_X	$logL_X$	χ^2/ν
–0.18	*–0.23*	*–0.28*	*+0.06*	*–0.19*	*+0.06*	*+0.01*	*–0.18*	*–0.36*	NLS1s
–0.00	–0.03	–0.01	–0.01	–0.01	+0.02	+0.05	+0.03	–0.09	BLS1s

[1]isted are the whole sample (110 objects), AGN with rest-frame 0.2-2.0 X-ray luminosity $logL_X > 37.0$ [W] (57), AGN with $logL_X < 37.0$ [W] (53), NLS1s (51), and BLS1s (59). Correlation with a Student's t-test >3.0 are displayed in bold face.

TABLE 2
RESULTS OF THE PCA

	EV-1	EV-2	EV-3	EV-4	EV-5	EV-6	EV-7	EV-8	EV-9	EV-10
Eigenvalue	3.1973	2.3228	1.2140	1.1593	0.8221	0.6378	0.3887	0.2494	0.0056	0.0028
Proportion	0.320	0.232	0.121	0.116	0.082	0.064	0.039	0.025	0.001	0.000
Cumulative	0.320	0.552	0.673	0.789	0.872	0.935	0.974	0.999	1.000	1.000
log FWHM(Hβ)	−0.358	+0.361	−0.134	−0.172	−0.110	+0.216	+0.490	−0.629	−0.007	−0.012
log FWHM([OIII])	+0.229	+0.195	−0.369	+0.422	−0.522	+0.399	+0.216	+0.342	+0.014	+0.003
log EW(Hβ)	−0.013	+0.453	+0.563	−0.251	−0.159	+0.187	−0.059	+0.267	−0.525	+0.056
log EW([OIII])	−0.393	−0.149	+0.461	+0.383	−0.122	+0.136	+0.009	+0.020	+0.220	−0.618
log EW(FeII)	+0.435	−0.032	+0.443	−0.027	+0.102	+0.459	+0.041	−0.192	+0.512	+0.303
log [OIII]/Hβ	−0.373	−0.343	+0.164	+0.457	−0.043	+0.053	+0.047	−0.092	−0.280	+0.643
log FeII/Hβ	+0.425	−0.349	−0.035	+0.122	+0.212	+0.286	+0.097	−0.319	−0.578	−0.331
α_X	+0.365	+0.059	+0.299	+0.209	−0.205	−0.650	+0.508	−0.088	−0.007	+0.005
log(L_X)	+0.139	+0.469	−0.021	+0.444	−0.030	−0.142	−0.594	−0.433	−0.028	−0.000
χ^2/ν	+0.055	−0.374	+0.042	−0.344	−0.758	−0.047	−0.292	−0.272	−0.008	−0.002

TABLE 3
SPEARMAN RANK ORDER CORRELATION COEFFICIENTS r_S AND STUDENT'S T-TEST VALUES t_S FOR THE FIRST TWO EIGENVECTORS WITH M_{BH}, L_X AND L/L_{Edd}.

	EV-1		EV-2	
	r_S	t_S	r_S	t_S
M_{BH}	–0.29	–3.20	+0.80	+14.0
L_X	+0.26	+2.78	+0.69	+9.83
L/L_{Edd}	+0.67	+9.38	–0.07	–0.71